JCTC Journal of Chemical Theory and Computation

Atom-Centered Density Matrix Propagation Calculations on the Methyl Transfer from CH_3Cl to NH_3: Gas-Phase and Continuum-Solvated Trajectories

Ashley N. Jay,† Kelly A. Daniel, and Eric V. Patterson*

Truman State University, Division of Science, 100 E. Normal St., Kirksville, Missouri 63501

Received September 8, 2006

Abstract: Atom-centered density matrix propagation (ADMP) calculations have been carried out to determine gas-phase and continuum-solvated (aqueous) trajectories for the Menshutkin reaction of methyl chloride with ammonia. The gas-phase trajectories reveal an exit channel that has not been previously reported. The aqueous trajectories give the expected results, indicating that solvated ADMP trajectories may be successfully computed using implicit solvation models. The solvated trajectories demonstrate the same stability and convergence qualities as the gas-phase trajectories.

Introduction

The Born−Oppenheimer approximation,[1] wherein the nuclear degrees of freedom are separated from the electronic degrees of freedom in the solution of the Schrödinger equation, has long been a centerpiece of quantum chemical calculations. While modern quantum chemical methods, particularly those employing density functional theory, efficiently provide accurate geometries and electronic energies for stationary points along a potential energy surface, the Born−Oppenheimer approximation eliminates all information about nuclear motion and its effect upon the potential energy surface. Thermodynamic parameters determined from harmonic vibrational analysis may be used to correct the electronic energies to enthalpies or free energies at a given temperature, yet the potential energy surface remains static. While the Born−Oppenheimer approximation has proved to be quite satisfactory, there are instances when it is necessary to account for nuclear motion and the effect it has on the potential energy surface.

In many circumstances, nuclear motion may be adequately described through classical mechanics. Fully classical methods, wherein the potential energy of the system is determined by a classical force field, have been used with great success.[2−7] For processes that require a quantum description of the potential energy, such as bond formation or dissociation, methods have been developed that combine a quantum chemical potential energy with classical propagation of the nuclear degrees of freedom, often collectively referred to as ab initio molecular dynamics (AIMD),[8] including the very popular Car−Parrinello methods,[9−11] Born−Oppenheimer MD,[12] and atom-centered density matrix propagation (ADMP).[13−15] While classical MD and AIMD methods are applicable to a wide variety of chemical problems, they are not appropriate for every case. If quantum effects such as tunneling or electronic excitations are known to be important, then the nuclei can no longer be treated as classical particles.[16−18] Of course, with the progression from fully classical to fully quantal approaches, the system size for efficient simulations dwindles from tens of thousands of atoms to two or three.

Given that most chemical reactions do not occur in the gas phase, it is important to account for solvation effects in order to accurately model a chemical process. Two limiting methods for applying solvation corrections exist: explicit solvation and implicit solvation. In the former, sufficient solvent molecules are added to the system to reproduce the effect of bulk solvation. Because of the size of the resulting supermolecular cluster, bulk explicit solvation is largely limited to classical MD. In principle, it is possible to use the bare minimum number of solvent molecules to reproduce

* Corresponding author e-mail: epatters@truman.edu.

† Former Truman State University undergraduate student. Current address: Department of Chemistry, University of Minnesota, Minneapolis.

10.1021/ct6002803 CCC: $37.00
Published on Web 01/24/2007

important stabilizing interactions, and this type of "microsolvation" has seen considerable use in MD simulations. Of course, care must be taken in the placement of the solvent molecules so that a balanced description of the entire potential energy surface is obtained.[7]

Implicit solvation models mimic bulk solvation effects through the use of a dielectric continuum or some similar means.[19] Continuum methods have seen wide use in the field of computational chemistry.[7,20] The advantage of continuum solvation is that it adds modestly to the cost of the computation. The primary disadvantage is that there is no way to recover structural information about the solvent molecules, so any structural role that the solvent plays in the course of a chemical reaction will remain undiscovered. A more subtle difficulty lies in the creation of the solute cavity within the continuum. Depending on how the cavity is constructed, numerical instabilities may arise for processes such as bond dissociation that significantly alter the shape of the cavity.[7]

A number of methods have been developed that seek to combine implicit and explicit solvation models to take advantage of the strengths of each. For example, it is possible to enclose a multilayered supermolecular cluster within a continuum model.[19] While this may be a reasonable thing to do, using the two theoretical approaches simultaneously combines not only their strengths but also their weaknesses. Multilayer methods, such as the popular ONIOM formalism,[21] reduce the computational time required to perform an explicitly solvated calculation by modeling the solvent at a lower level of theory than the solute. The combination of ONIOM with ADMP has been reported in the literature using a development version of Gaussian 03.[22]

Among the more promising recent developments in AIMD is the ADMP method.[13−15] The primary advantage of ADMP is that it provides results similar in accuracy with Born−Oppenheimer MD[12] but at a substantially reduced computational cost. Recent applications of ADMP demonstrate the accuracy and efficiency of the method.[22−31] Given the promise of ADMP, it is worthwhile to explore whether accurate solvated trajectories can be obtained simply by applying a standard continuum solvation model. If so, the combined efficiencies of ADMP and continuum solvation could make it possible to determine solvated dynamic trajectories for reasonably large systems where structural data regarding the solvent are not essential. In fact, a recent study demonstrated the reliability of ADMP coupled with the conductor-like polarizable continuum model (CPCM) in a mixed explicit/implicit solvent system.[32] Even greater efficiency and flexibility could be obtained if no explicit solvent molecules were used. Therefore, we have chosen to explore ADMP in conjunction with the integral equation formalism−polarizable continuum model (IEF−PCM) solvation model[33] in the absence of any explicit solvent. Furthermore, both have been used as implemented in the standard binary release of Gaussian 03,[34] meaning no code modifications are necessary.

To test the general applicability of the ADMP/IEF−PCM combination, trajectories for the S_N2 Menschutkin reaction[35,36] of ammonia with methyl chloride have been determined in both the gas phase and in aqueous solution. This reaction was chosen since it is well-known to have exceptionally different gas-phase and solution-phase potential energy surfaces. Accordingly, the ADMP/IEF−PCM combination should produce dramatically different trajectories than those determined in the gas phase. Menshutkin reactions in general have been extensively studied experimentally,[36] and the specific reaction explored herein has been the subject of a number of theoretical studies.[37−48] Early simulations of the reaction pathway employed statistical trajectory[37] and Monte Carlo calculations[38] in an explicit water solvent; however a symmetry constraint was employed to keep the N, C, and Cl atoms collinear. A study employing second-order reaction path following in conjunction with the implicit generalized conductor-like screening model water model examined the trajectory with no symmetry constraint.[44] Monte Carlo simulations in implicit solvent have also been performed,[48] as have continuum-solvated[46] and microsolvated[45] variational transition state calculations, which can account for quantum-mechanical tunneling. The consensus of this previous work is that the gas-phase reaction has a barrier of approximately 30 kcal/mol and an overall energy change of approximately 117 kcal/mol, in excellent agreement with the experimental value of 111 ± 5 kcal/mol.[49] In aqueous solution, the consensus barrier height is approximately 25 kcal/mol, while the overall reaction is now exothermic by approximately 20 kcal/mol. There is some variability in these latter numbers, due in no small part to the various approximations employed in the different studies. The reaction with methyl bromide in place of methyl chloride has also been examined computationally,[50,51] with similar results.

In the current work, we report ADMP trajectory calculations for the Menschutkin reaction of ammonia with methyl chloride in both the gas phase and an implicit aqueous solution. Previously, ADMP has been shown to work well with CPCM for studying the solvation energy of chloride anions in aqueous solution.[32] We now show that continuum-solvated ADMP trajectories are equally suited for the study of nucleophilic reactions in aqueous solution. While the primary purpose of the current work is to explore the stability of continuum-solvated ADMP trajectories for computing nucleophilic reaction pathways, the data have revealed a novel product channel in the gas phase. The present results demonstrate that ADMP may be reliably paired solely with a continuum solvation model for the exploration of solvated reaction dynamics. The combination of these two efficient methods holds great promise for the study of larger and more complex systems than the simple test case presented herein.

Computational Methods

Stationary-point geometries were determined using the MPW1K hybrid density functional[52] and the MIDIY+ basis set,[53] both due to the Truhlar group. This combination was chosen as it has been shown to provide excellent estimates for forward and reverse barrier heights while still giving good results for overall energy changes during the course of a chemical reaction.[53] Furthermore, MPW1K has performed well for capturing nonbonded interactions.[54] Aqueous-phase

geometries were optimized using the IEF−PCM of Tomasi.[33] The all-atom UFF topological model was used in place of the default united-atom UA0 topological model in order to avoid difficulties with proton dissociation. All other default parameters for an aqueous solvent were employed. Harmonic frequencies were determined for all stationary points to ascertain the correct number of imaginary eigenvalues (i.e., 0 for minima and 1 for transition states). Intrinsic reaction coordinate calculations[55] were employed to confirm that each transition state connects to the minima as described below.

Given that noncovalent complexes figure heavily in the potential energy surface for this reaction (see below), the quality of the MPW1K results was checked against results obtained from second-order Møller−Plesset theory.[56] All stationary points were reoptimized at the MP2/MIDIY+ level of theory, both in the gas phase and in aqueous solution as described above. In every case, the results from the MPW1K calculations compare favorably with the MP2 results, yielding relative energies of the stationary points that differ by less than 1 kcal/mol in most cases (see the Supporting Information). Thus, we have confidence that the MPW1K density functional captures noncovalent interactions with accuracy similar to that of MP2, and trajectories computed at the MPW1K/MIDIY+ level should reliably sample the potential energy surfaces of the gas-phase and solvated reactions.

ADMP trajectories[13−15] were initiated from both the gas-phase and solution-phase transition states for backside nucleophilic attack. The MPW1K/MIDIY+ level of theory was employed for the ADMP calculations as described above for the stationary-point calculations. A time step of 0.25 fs was used for the majority of the trajectories, while the default time step of 0.1 fs was required in a few cases. The default fictitious electron mass of 0.1 amu was used throughout. A thermostat was employed to maintain a constant temperature of 298 K.[57,58] A total of 100 random trajectories were determined in each phase. Each trajectory was integrated for a minimum of 200 fs, with more data collected as necessary (see below). A smaller number of trajectories was initiated from other reactant complexes.

All calculations were performed with the standard binary release of G03M.[34]

Results and Discussion

Given that no zero-point or thermal corrections are applied during the determination of an ADMP trajectory, all discussion will be limited to relative self-consistent field energies with no further correction. Standard corrections are provided in the Supporting Information.

Stationary Points. Selected geometries and relative energies are presented in Figure 1. The complete set of stationary-point data is available in the Supporting Information.

As is typical of S_N2 reactions in the gas phase, separated reactants initially collapse to an ion-dipole complex that is 2.3 kcal/mol lower in energy than the reactants. This proceeds to a transition state with a relative energy of 32.0 kcal/mol, which continues to an ion-dipole product complex that lies 30.6 kcal/mol above isolated starting materials. The isolated ionic products are found to be 117.0 kcal/mol higher in energy than the reactants, indicating an impossibly unfavorable reaction in the gas phase. These results are all in substantial agreement with previous experimental[49] and theoretical[37−48] studies on this system. A much lower-energy hydrogen-bonded product complex, which has not been previously reported, is found to be 9.7 kcal/mol below starting materials. In this complex, the chlorine and amine share the acidic proton in a nearly equitable fashion (Figure 1). Of course, to reach this minimum, the chloride has to migrate a significant distance from its location in the ion-dipole product complex, implying that the minimum energy reaction pathway may not involve complete dissociation to the ionic products. Complete abstraction of this proton by chloride would lead to a charge-neutral product pair (methylamine plus hydrogen chloride), which is 5.6 kcal/mol higher in energy than the separated reactants.

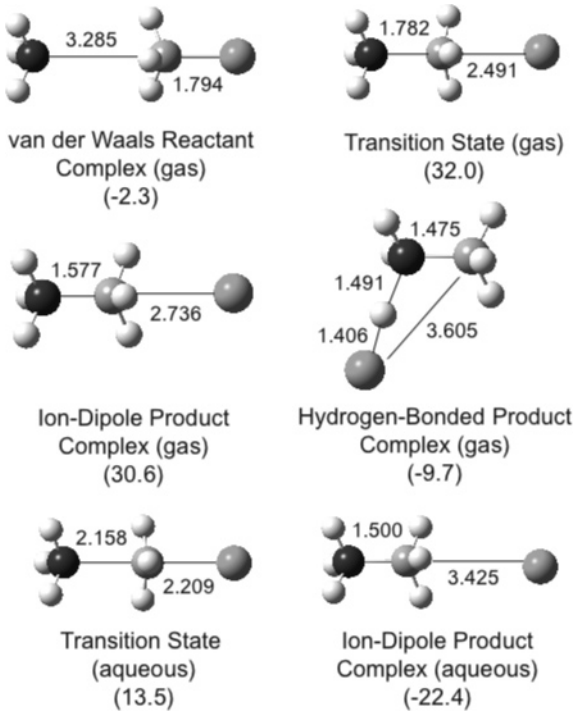

Figure 1. Stationary point geometries and important bond lengths (Å) for selected species considered in this study. Electronic energies relative to separated reactants are given in parenthesis (kcal/mol).

The aqueous-phase relative energies are also in good agreement with previously published work.[37,38,40−42,44−48] The transition state for attack is found 13.5 kcal/mol above isolated reactants and leads to an ion-dipole product complex 22.4 kcal/mol below the reactants (no van der Waals reactant complex could be located in the aqueous phase). Separated ionic products are nearly isoenergetic with the ion-dipole product complex, while the charge-neutral product pair is 6.1 kcal/mol higher in energy than the reactants. No aqueous-phase stationary point corresponding to the hydrogen-bonded complex could be located. Thus, the aqueous reaction closely resembles a textbook example of an exothermic S_N2 mechanism, and the ionic products are predicted to be quite favorable.

It is instructive to examine the differences between corresponding gas-phase and solution-phase structures. It has been suggested that, in general, the differences in geometry

Table 1. Important Bond Distances and Total Energies of Selected Gas-Phase and Aqueous-Phase Geometries

	bond distance[a]		PCM E(SCF)[b] (ΔG_{solv})[c]	
species	gas phase	aqueous phase	gas-phase geometry	aqueous-phase geometry
		Methyl Chloride		
C−Cl	1.788	1.800	−497.77868 (0.4)	−497.77874 (0.4)
		Ion-Dipole Reactant Complex		
C−Cl	1.794	N/A	−554.02853 (2.1)	N/A
C−N	3.285	N/A		
		TS		
C−Cl	2.491	2.209	−554.03120 (−35.0)	−554.00889 (−11.1)
C−N	1.782	2.158		
		Ion-Dipole Product Complex		
C−Cl	2.736	3.425	−554.05526 (−48.7)	−554.06601 (−62.7)
C−N	1.577	1.500		
		Hydrogen-Bonded Product Complex		
C−N	1.475	N/A	−554.05037 (−5.3)	N/A
N−H	1.491	N/A		
H−Cl	1.406	N/A		
		Methylammonium		
C−N	1.512	1.497	−95.78453 (−65.8)	−95.78470 (−66.1)
		Methylamine		
C−N	1.466	1.473	−95.32144 (−0.2)	−95.32163 (−0.4)

[a] Units of angstroms. [b] Units of hartrees. [c] Units of kcal/mol.

between the gas phase and solution phase are insignificant enough that applying solvation corrections to gas-phase geometries is sufficient and that the extra computational expense associated with determining solution-phase geometries would be time wasted. Geometric data is provided in Figure 1 and summarized in Table 1, which also provides a comparison between the self-consistent field (SCF) and free energies of solvation from single-point IEF−PCM calculations on the gas-phase structures to the corresponding energies of the solution-phase structures.

An examination of Table 1 reveals that the bond distances for the minima vary by less than 1% between the gas-phase and solution-phase structures for minimum-energy species. Similarly, the IEF−PCM SCF energies agree within 0.1 kcal/mol for these same species. However, there are dramatic differences in the transition state structures, where the bond distances differ by 11% for the C−Cl bond and 17% for the C−N bond and the energies differ by 14 kcal/mol. The gas-phase transition state structure more closely resembles products than does the solution-phase transition state. This trend has been observed previously for this reaction[37,38,41,42,44−46,48] and is as predicted by the Hammond Postulate.[59] Clearly, then, if the single-point solvation corrections on the gas-phase transition state structure had been used to predict the barrier for this particular reaction, the barrier would have been underestimated by a significant margin. It would, in fact, be estimated to have a barrier of −0.7 kcal/mol (the IEF−PCM SCF energy for the gas-phase ammonia structure is −56.25144 hartrees). The same general conclusion is reached if the free energies of solvation, which are given in parentheses under the SCF energies in Table 1, are examined. A similar trend is seen for the initial ion-dipole product complex, except that the aqueous geometry is now more highly solvated than the gas-phase geometry. While the reaction under study is a severe test due to the ionic nature of the products, it is clear that a good degree of caution must be exercised when estimating solvated surfaces using gas-phase transition state structures.

Chart 1

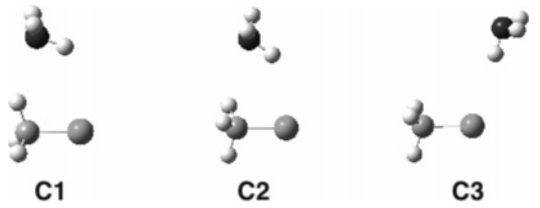

Alternate modes of nucleophilic attack were considered. A series of relaxed potential energy surface scans was conducted in both the gas-phase and solution, fixing either the N−C distance or the N−Cl distance while systematically altering the N−C−Cl angle. In this way, concentric potential energy plots were constructed at N−C and N−Cl distances ranging from 2.0 to 4.5 Å at 0.5 Å steps. These scans led to the discovery of additional noncovlant reaction complex stationary points, shown in Chart 1 (details are provided in the Supporting Information). In the gas phase, **C1** was found to be a minimum while **C2** is a transition state for methyl rotation leading to **C1**. In the aqueous phase, **C1** is found to be a third-order saddle point while **C3** is a second-order saddle point. These imaginary modes correspond to methyl rotations, rotations of the ammonia moiety relative to the substrate, or slipping of the nucleophile along the van der Waals contact radius. Complex **C1** is not a stationary point in aqueous solvent, while **C3** is not a stationary point in the gas phase. In the gas phase, complexes **C1** and **C2** are essentially isoenergetic with the hydrogen-bonded reactant complex discussed above. In the aqueous phase, complexes **C1** and **C3** are essentially isoenergetic with separated reactants. Thus, there is predicted to be a very flat potential energy profile for the nucleophile orbiting the substrate in both phases, and attack could potentially initiate from any direction.

Accordingly, several attempts were made to locate additional attack transition states for approach of the nucleophile. A relaxed potential energy surface scan starting with **C1** and forcing the N−C bond distance to become shorter did eventually lead to the formation of the hydrogen-bonded product complex shown in Figure 1. However, the activation barrier along this pathway was estimated to be greater than 50 kcal/mol. Furthermore, every attempt to optimize a transition state along this pathway failed, with the optimizations reverting to complex **C1**. Similar calculations beginning from **C2** and **C3** yield the same result. Likewise, no attack transition states could be located from any of the three complexes when shrinking the N−Cl distance. Therefore, the only confirmed attack transition states are the traditional S_N2 backside attack transition states discussed above (Figure 1). It appears clear, then, that stationary-point calculations predict only a single entrance channel for this reaction.

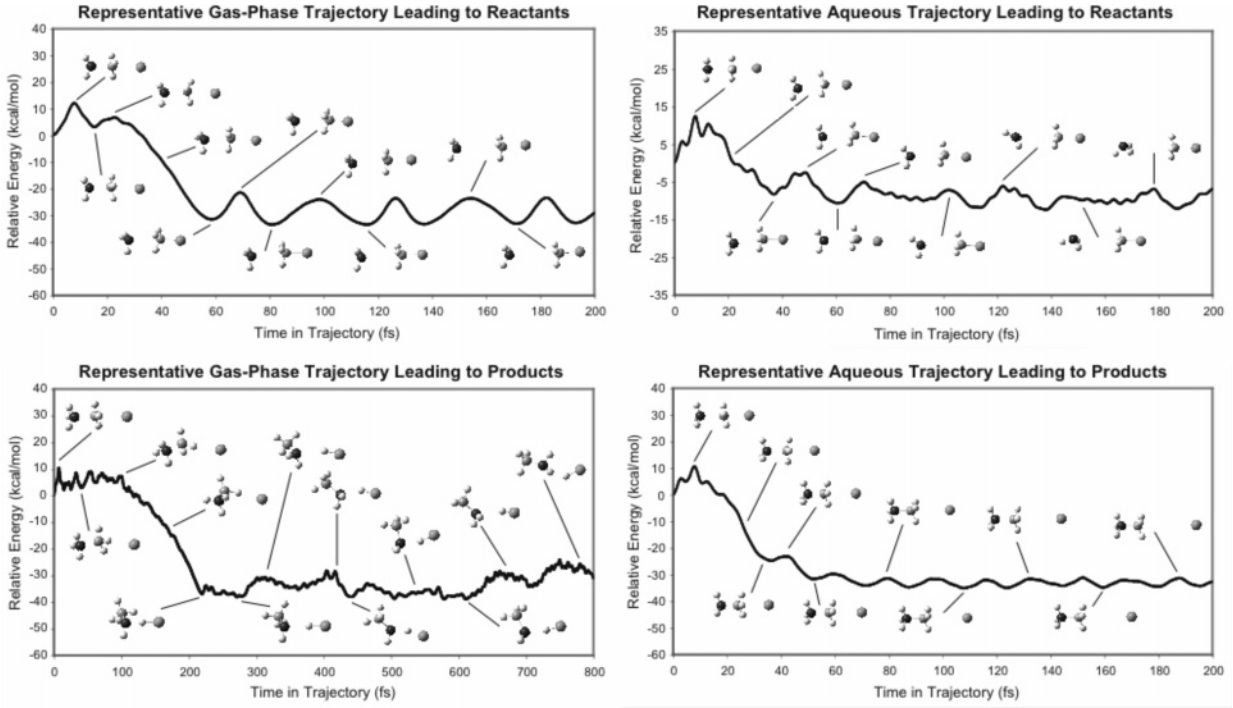

Figure 2. Representative trajectories in the gas and aqueous phases and selected geometries along each trajectory.

Trajectory Calculations. A total of 100 random trajectories were initiated each in the gas and aqueous phases, starting from the transition state stationary structures. Of the gas-phase trajectories, six failed to complete, while seven failed in the aqueous phase. The remaining trajectories were characterized as progressing toward products or reactants by visualizing the results in GaussView[60] and analyzing the changes in the C−N and C−Cl bond distances. Representative trajectories are presented in Figure 2, while a typical bond distance analysis is provided in Figure 3.

Gas-Phase Trajectories. Of the gas-phase trajectories, 84% returned to separated starting materials while 16% proceeded to the hydrogen-bonded product complex. None were found to lead to complete dissociation to ionic products. Those that returned to reactants did so quickly, with the C−N bond distance exceeding that found in the van der Waals reactant complex no later than 120 fs into the trajectory. By the end of 200 fs, the C−N bond distance exceeds 4.5 Å while the C−Cl distance has settled into an oscillation about the equilibrium bond distance as determined by the stationary-point calculations (Figure 3). The potential energy has settled on a value around 30 kcal/mol below the transition state (Figure 2), as is expected from the stationary point data presented in Figure 1.

Much more interesting to consider is the fate of those gas-phase trajectories that formed the hydrogen-bonded complex. In the typical example shown in Figure 2, the chloride appears to be dissociating rapidly by 50 fs. However, between 100 and 200 fs, the chloride completes a partial orbit of the methylammonium moiety and is positioned to abstract a proton from the nitrogen. Given the unusual nature of these product trajectories, they were continued for an additional 600 fs to give a total of 800 fs in the trajectory. During this

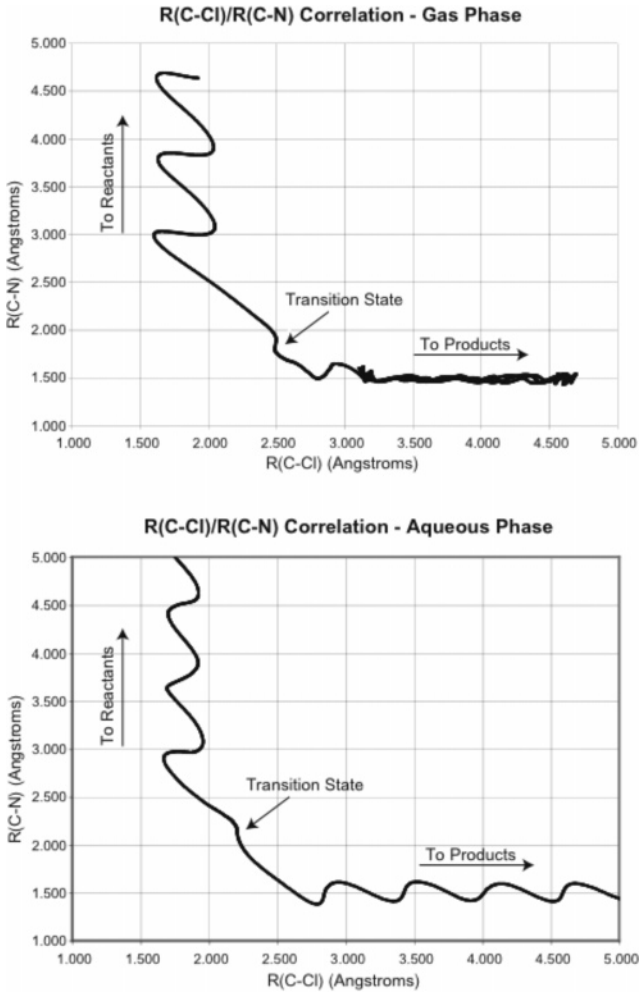

Figure 3. Correlation of C−Cl and C−N bond distances for those trajectories presented in Figure 2.

additional simulation time, the hydrogen-bonded complex never dissociates but is quite dynamic. When the product quadrant of the gas-phase plot in Figure 3 is examined, it can be seen that the C−Cl bond distance fluctuates between 3.5 and 4.7 Å while the C−N bond distance remains nearly constant at 1.5 Å. The potential energy has settled on a value nearly 40 kcal/mol below the transition state, which agrees well with the relative energy of the separated products (see above).

A trajectory of this sort has never been reported for this reaction and indicates that there may be a viable product channel available at 298 K. It is noteworthy that the potential energy appears to be rising over the last 150 fs of the 800 fs simulation, which may indicate that additional dissociation is occurring. Accordingly, one trajectory was integrated for a total of 2 ps. Indeed, between 900 and 1400 fs, the complex becomes much more dynamic, leading to dissociation by 1600 fs. By the end of the 2 ps trajectory, the methylamine and hydrogen chloride molecules have separated by more than 9 Å (see the Supporting Information).

Aqueous Trajectories. In the aqueous simulations, 52% of the trajectories returned to separated reactants while 48% continued to separated ionic products. None remained associated in any way or followed an unexpected trajectory as discussed above for the gas-phase simulations. Those trajectories that returned to reactants did so at a slightly faster pace than seen in the gas-phase simulation, with the C−N bond distance exceeding 3.5 Å by 100 fs. By 150 fs, there is little interaction between the two fragments and the lone pair of the ammonia is no longer oriented coincident with the C−Cl axis. By the end of the 200 fs simulation, the C−N bond distance has exceeded 5 Å while the C−Cl distance has settled into an oscillation about 1.7 Å (Figure 3), and the energy has settled on the expected value (Figure 2). There are few significant differences between those gas-phase and aqueous-phase trajectories that return to reactants.

The aqueous-phase product trajectories are dramatically different from the gas-phase product trajectories. First, similar numbers of aqueous trajectories follow the product and reactant channels, which is reasonable given that both the products and reactants are steeply downhill from the transition state. This contrasts with the gas-phase results, where the vast majority of the trajectories return to reactants. Second, the aqueous product trajectories rapidly expel the chloride ion and form the expected ionic products with no intervention of ion-dipole or hydrogen-bonded complexes. The chloride is effectively expelled within 100 fs, and the C−Cl distance exceeds 5 Å by the end of the 200 fs simulation, while the C−N bond distance and potential energy oscillate around their expected values (Figures 2 and 3).

Alternative Trajectories. In addition to the trajectories discussed above, which all originated from the traditional S_N2 backside attack transition states, a limited number of trajectories were initiated from complexes **C1**, **C2**, and **C3** (see above). Regardless of solvation, the general finding from these trajectories is that the nucleophile remains within van der Waals contact of the substrate or drifts away to separated reactants. In no case was an attack trajectory observed. We therefore conclude that the backside attack trajectories discussed above are the only energetically feasible reaction manifold for this system under the specific conditions considered.

Stability of Simulations. Several parameters may be considered when determining whether a simulation has remained stable. First, smooth fluctuations in energy and geometric parameters as indicated in Figures 2 and 3 show that there are no discontinuities. This is particularly important to note for the solvated trajectories, where it is reasonable to be concerned about fluctuations in the shape and size of the solute cavity. The continuous results indicate that those concerns are unfounded, at least on the time and distance scale considered in this work. For 10 of the 100 aqueous trajectories, a step size of 0.1 fs was required to obtain smoothly continuous results. Even with reduced step sizes, a handful of trajectories failed. A total of seven aqueous- and six gas-phase trajectories failed to propagate smoothly. The fact that the failure rate is nearly identical for the aqueous- and gas-phase trajectories implies that the reason for failure has little to do with the solvation model and is more likely due to the initial random velocities leading to unstable results.

In addition to the qualitative measures just described, the quality of a trajectory can be evaluated on theoretical grounds by examining the change of the fictitious Hamiltonian with respect to time, the idempotency, and ensuring proper initial conditions for the kinetic energy. With respect to the first two, there is no discernible difference in the Hamiltonian traces or idempotency of the gas-phase and aqueous trajectories, and all are well within acceptable limits.[14] Such stability of ADMP simulations in a continuum solvent has been previously demonstrated.[32] In order to ensure that the simulation remains on the ground-state electronic surface, initial conditions must be chosen such that the supplied kinetic energy is much less than the highest occupied molecular orbital−lowest unoccupied molecular orbital (HOMO−LUMO) gap. For these simulations, the initial kinetic energy is 0.011 hartrees, while the HOMO−LUMO gap in the transition state structures is approximately 0.3 hartrees.

Conclusions

In one of the first applications of its type, ADMP trajectory simulations have been coupled with the IEF−PCM implicit solvation model to successfully simulate the Menschutkin reaction of ammonia with methyl chloride. It is gratifying that there are no surprises in the aqueous-phase trajectories and that the solvated simulations are just as stable as the gas-phase simulations, as has been previously shown for the simulation of chloride anions in aqueous solution.[32] It is clear that the combination of ADMP and IEF−PCM has efficiently and accurately modeled the potential energy surface for the reaction of ammonia with methyl chloride. The aqueous product trajectories are dramatically different from the gaseous product trajectories, as is expected. It is readily apparent that ADMP/IEF−PCM simulations may be useful when solvation is essential, but detailed structural information about explicit solvent molecules is not, and when computational efficiency is of concern.

Acknowledgment. The authors thank Truman State University for supporting this research.

Supporting Information Available: Stationary point geometries and their associated energies and data for the 2 ps gas-phase trajectory leading to methylamine and hydrogen chloride. This material is available free of charge via the Internet at http://pubs.acs.org.

References

(1) Born, M.; Oppenheimer, R. *Ann. Phys.* **1927**, *84*, 457−484.

(2) Brooks, C. L., III; Case, D. A. *Chem. Rev.* **1993**, *93*, 2487−2502.

(3) Cheatham, T. E., III; Brooks, B. R. *Theor. Chem. Acc.* **1998**, *99*, 279−288.

(4) Beveridge, D. L.; McConnell, K. J. *Curr. Opin. Struct. Biol.* **2000**, *10*, 182−196.

(5) Adcock, S. A.; McCammon, J. A. *Chem. Rev.* **2006**, *106*, 1589−1615.

(6) Jensen, F. *Introduction to Computational Chemistry*; John Wiley and Sons: Chichester, U. K., 1999; pp 6−51.

(7) Cramer, C. J. *Essentials of Computational Chemistry: Theories and Models*, 2nd ed.; John Wiley and Sons Ltd: West Sussex, England, 2004; pp 69−102, 385−455.

(8) Marx, D.; Hutter, J. In *Procedings of Modern Methods and Algorithms of Quantum Chemistry, Julich*; Grotendorst, E., Ed.; John von Neumann Institute for Computing: Jülich, Germany, 2000.

(9) Car, R.; Parrinello, M. *Phys. Rev. Lett.* **1985**, *55*, 2471−2474.

(10) Hartke, B.; Carter, E. A. *J. Chem. Phys.* **1992**, *97*, 6569−6578.

(11) Lippert, G.; Hutter, J.; Parrinello, M. *Theor. Chem. Acc.* **1999**, *103*, 124−140.

(12) For a discussion of several recent developments in this field, see: *Modern Methods for Multidimensional Dynamics Computation in Chemistry*; Thompson, D. L., Ed.; World Scientific: Singapore, 1998.

(13) Schlegel, H. B.; Millam, J. M.; Iyengar, S. S.; Voth, G. A.; Daniels, A. D.; Scuseria, G. E.; Frisch, M. J. *J. Chem. Phys.* **2001**, *114*, 9758−9763.

(14) Iyengar, S. S.; Schlegel, H. B.; Millam, J. M.; Voth, G. A.; Scuseria, G. E.; Frisch, M. J. *J. Chem. Phys.* **2001**, *115*, 10291−10302.

(15) Schlegel, H. B.; Iyengar, S. S.; Li, X.; Millam, J. M.; Voth, G. A.; Scuseria, G. E.; Frisch, M. J. *J. Chem. Phys.* **2002**, *117*, 8694−8704.

(16) Jungwirth, P.; Gerber, R. B. *Chem. Rev.* **1999**, *99*, 1583−1606.

(17) Jasper, A. W.; Nangia, S.; Zhu, C.; Truhlar, D. G. *Acc. Chem. Res.* **2006**, *39*, 101−108.

(18) Fernández-Ramos, A.; Miller, J. A.; Killenstein, S. J.; Truhlar, D. G. *Chem. Rev.* **2006**, *106*, 4518−4584.

(19) Tomasi, J.; Mennucci, B.; Cammi, R. *Chem. Rev.* **2005**, *105*, 2999−3093.

(20) Cramer, C. J.; Truhlar, D. G. *Chem. Rev.* **1999**, *99*, 2160−2200.

(21) Vreven, T.; Morokuma, K. *J. Comput. Chem.* **2000**, *21*, 1419−1432.

(22) Rega, N.; Iyengar, S. S.; Voth, G. A. *J. Phys. Chem. B* **2004**, *108*, 4210−4220.

(23) Sailer, W.; Pelc, A.; Limao-Vieira, P.; Mason, N. J.; Limtrakul, J.; Scheier, P.; Probst, M.; Mark, T. D. *Chem. Phys. Lett.* **2003**, *381*, 216−222.

(24) Tian, W. Q.; Wang, Y. A. *J. Chem. Theory Comput.* **2005**, *1*, 353−362.

(25) Iyengar, S. S. *J. Chem. Phys.* **2005**, *123*, 084310/9.

(26) Liu, L. V.; Tian, W. Q.; Wang, Y. A. *J. Phys. Chem. B* **2006**, *110*, 13037−13044.

(27) Joubert, L.; Adamo, C. *J. Chem. Phys.* **2005**, *123*, 211103/1−211103/4.

(28) Iyengar, S. S.; Petersen, M. K.; Day, T. J. F.; Burnham, C. J.; Teige, V. E.; Voth, G. A. *J. Chem. Phys.* **2005**, *123*, 084309/1−084309/9.

(29) Zhang, L.; Li, H.; Hu, X.; Shijuin, H. *J. Phys. Chem. A* **2006**, *110*, 7690−7695.

(30) Ciofini, I.; Adamo, C. *J. Mol. Struct.* **2006**, *762*, 133−137.

(31) Joubert, L.; Pavone, M.; Barone, V.; Adamo, C. *J. Chem. Theory Comput.* **2006**, *2*, 1220−1227.

(32) Rega, N.; Brancato, G.; Barone, V. *Chem. Phys. Lett.* **2006**, *422*, 367−371.

(33) Cances, E.; Mennucci, B.; Tomasi, J. *J. Chem. Phys.* **1997**, *107*, 3032−3041.

(34) Frisch, M. J.; Trucks, G. W.; Schlegel, H. B.; Scuseria, G. E.; Robb, M. A.; Cheeseman, J. R.; Montgomery, J. A., Jr.; Vreven, T.; Kudin, K. N.; Burant, J. C.; Millam, J. M.; Iyengar, S. S.; Tomasi, J.; Barone, V.; Mennucci, B.; Cossi, M.; Scalmani, G.; Rega, N.; Petersson, G. A.; Nakatsuji, H.; Hada, M.; Ehara, M.; Toyota, K.; Fukuda, R.; Hasegawa, J.; Ishida, M.; Nakajima, T.; Honda, Y.; Kitao, O.; Nakai, H.; Klene, M.; Li, X.; Knox, J. E.; Hratchian, H. P.; Cross, J. B.; Bakken, V.; Adamo, C.; Jaramillo, J.; Gomperts, R.; Stratmann, R. E.; Yazyev, O.; Austin, A. J.; Cammi, R.; Pomelli, C.; Ochterski, J. W.; Ayala, P. Y.; Morokuma, K.; Voth, G. A.; Salvador, P.; Dannenberg, J. J.; Zakrzewski, V. G.; Dapprich, S.; Daniels, A. D.; Strain, M. C.; Farkas, O.; Malick, D. K.; Rabuck, A. D.; Raghavachari, K.; Foresman, J. B.; Ortiz, J. V.; Cui, Q.; Baboul, A. G.; Clifford, S.; Cioslowski, J.; Stefanov, B. B.; Liu, G.; Liashenko, A.; Piskorz, P.; Komaromi, I.; Martin, R. L.; Fox, D. J.; Keith, T.; Al-Laham, M. A.; Peng, C. Y.; Nanayakkara, A.; Challacombe, M.; Gill, P. M. W.; Johnson, B.; Chen, W.; Wong, M. W.; Gonzalez, C.; Pople, J. A. *Gaussian 03M*, revision C.02; Gaussian, Inc.: Wallingford, CT, 2004.

(35) Menshutkin, N. *Z. Phys. Chem.* **1890**, *5*, 589.

(36) Abboud, J.-L. M.; Notario, R.; Bertran, J.; Sola, M. *Prog. Phys. Org. Chem.* **1993**, *19*, 1−182.

(37) Gao, J. *J. Am. Chem. Soc.* **1991**, *113*, 7796−7797.

(38) Gao, J.; Xia, X. *J. Am. Chem. Soc.* **1993**, *115*, 9667−9675.

(39) Shaik, S.; Ioffe, A.; Reddy, A. C.; Pross, A. *J. Am. Chem. Soc.* **1994**, *116*, 262−273.

(40) Maran, U.; Pakkanen, T. A.; Karelson, M. *J. Chem. Soc., Perkin Trans. 2* **1994**, 2445−2452.

(41) Dillet, V.; Rinaldi, D.; Bertrán, J.; Rivail, J.-L. *J. Chem. Phys.* **1996**, *104*, 9437−9444.

(42) Fradera, X.; Amat, L.; Torrent, M.; Mestres, J.; Constans, P.; Besalú, E.; Matrí, J.; Simon, S.; Lobato, M.; Oliva, J. M.; Luis, J. M.; Andrés, J. L.; Solà, M.; Carbó, R.; Duran, M. *J. Mol. Struct.* **1996**, *371*, 171−183.

(43) Maran, U.; Karelson, M.; Pakkanen, T. A. *J. Mol. Struct.* **1997**, *397*, 262−272.

(44) Truong, T. N.; Truong, T.-T. T.; Stefanovich, E. V. *J. Chem. Phys.* **1997**, *107*, 1881−1889.

(45) González-Lafont, A.; Jordi, V.; Lluch, J. M.; Bertrán, J.; Steckler, R.; Truhlar, D. G. *J. Phys. Chem. A* **1998**, *102*, 3420−3428.

(46) Chuang, Y.-Y.; Cramer, C. J.; Truhlar, D. G. *Int. J. Quantum Chem.* **1998**, *70*, 887−896.

(47) Amovilli, C.; Mennucci, B.; Floris, F. M. *J. Phys. Chem. B* **1998**, *102*, 3023−3028.

(48) Castejon, H.; Wiberg, K. B. *J. Am. Chem. Soc.* **1999**, *121*, 2139−2146.

(49) Pedley, J. B. *Thermochemical Data and Structures of Organic Compounds*; Thermodynamics Research Center: College Station, TX, 1994; Vol. 1.

(50) Sola, M.; Lledos, A.; Duran, M.; Bertran, J.; Abboud, J.-L. M. *J. Am. Chem. Soc.* **1991**, *113*, 2873−2879.

(51) Gordon, M. S.; Freitag, M. A.; Bandyopadhyay, P.; Jensen, J. H.; Kairys, V.; Stevens, W. J. *J. Phys. Chem. A* **2001**, *105*, 293−307.

(52) Zhao, Y.; Truhlar, D. G. *J. Phys. Chem. A* **2004**, *108*, 6908−6918.

(53) Lynch, B. J.; Truhlar, D. G. *Theor. Chem. Acc.* **2004**, *111*, 335−344.

(54) Zhao, Y.; Schultz, N. E.; Truhlar, D. G. *J. Chem. Theory Comput.* **2006**, *2*, 364−382.

(55) Gonzales, C.; Schlegel, H. B. *J. Chem. Phys.* **1989**, *90*, 2154.

(56) Møller, C.; Plesset, M. S. *Phys. Rev.* **1934**, *46*, 618−622.

(57) Nosé, S. *J. Chem. Phys.* **1984**, *81*, 511−519.

(58) Hoover, W. G. *Phys. Rev. A: At., Mol., Opt. Phys.* **1985**, *31*, 1695−1697.

(59) Hammond, G. S. *J. Am. Chem. Soc.* **1955**, *77*, 334−338.

(60) Dennington, R., II; Keith, T.; Millam, J. M.; Eppinnett, K.; Hovell, W. L.; Filliland, R. *GaussView*; Semichem, Inc.: Shawnee Mission, KS, 2003.

CT6002803